Structure-Dependent Balance between Excited-State Deactivation Pathways in Cross-Conjugated Molecular Photoswitches

Luke R. O'Connor,[1] Nicholas P. Adams, [1] Chana R. Honick, [1] Yuqi Song,[1] Neal Haldar,[2] J. D. Tovar, [1,3,4] and Arthur E. Bragg[1]*

1 Department of Chemistry, Johns Hopkins University, 3400 N. Charles St., Baltimore, MD 21218 U.S.A.

2 Department of Chemistry, University of California, Berkeley, Berkeley, CA 94720-1460 U.S.A.

3 Institute of NanoBioTechnology, Johns Hopkins University, 3400 N. Charles St., Baltimore, MD 21218 U.S.A.

4 Department of Materials Science and Engineering, Johns Hopkins University, 3400 N. Charles St., Baltimore, MD 21218, U.S.A.

Abstract: Diaryl thieno-[3,4-*b*]thiophenes (TT) are photoswitchable compounds that operate through reversible photoinduced cyclization/cycloreversion and have been designed specifically for integrating within π-conjugated polymers to switchably manipulate polymer electronic properties. Here we report on how cross conjugating the central TT moiety impacts photocyclization dynamics as interrogated using transient absorption spectroscopies (TAS) for a series of switches built with electron-rich substituents that have various electronic interaction strengths with the TT core. For cross-conjugated structures exhibiting a propensity to switch in steady-state photoconversion experiments, ultrafast TAS reveals signatures of rapid dynamics (occurring within <1-10 ps) similar to those observed for unsubstituted switches and that are consistent with photocyclization. In contrast, TAS reveals comparatively slower spectral dynamics (~100 ps) that are not consistent with cyclization for switches that are cross-conjugated with substituents that have greater electronic interaction with the TT core and that exhibit no propensity to photoswitch in photoconversion experiments. Microsecond TAS confirms that photoinduced cyclization occurs for the former and that a metastable triplet state localized on the conjugated backbone is generated with the latter. We find that the balance of these two deactivation pathways is sensitive to the interaction strength of the conjugated substituents with the core, with select structures exhibiting signatures of both. These findings are consistent with prior work demonstrating that the LUMO character is delocalized over the switch backbone when there are strong interactions with cross-conjugating groups and reveal that the competition between deactivation pathways can be controlled structurally by weakening π conjugation across the backbone.

TOC Graphic:

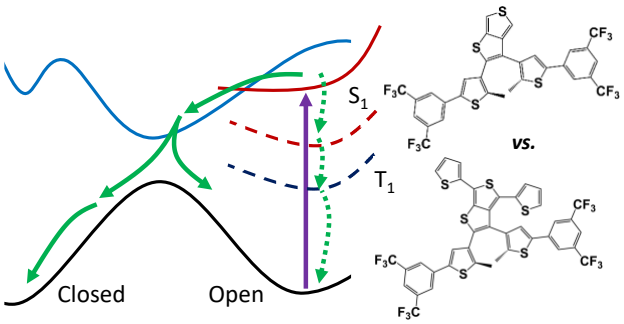

Introduction

Light triggers important natural processes, including photosynthesis,[1] fundamental processes underlying vision,[2] and the generation of vitamin D in the body.[3] There is great interest in using light to generate and control material responses with the same success as nature in order to establish innovative ways for manipulating material properties and function.[4-8] It is for this reason that photoswitches, a class of material that undergo changes in structure or chemical properties upon photoexcitation, have been explored extensively for applications including, but not limited to, contrast control for fluorescent imaging of biological systems,[9-10] readable and writable optical memory,[5] photoacidity,[11] metal-ion and pH sensing,[12-13] light-controlled catalysis,[14] switchable electrical conductivity and photovoltaic properties,[8, 15-17] and photoactivated mechanical actuation.[18] In this contribution, we present on the photochemical dynamics of cross-conjugated diaryl thieno-[3,4-*b*]thiophenes (TT), which are model systems for using light-switchable motifs to manipulate electronic properties of pi-conjugated oligomers and polymers.[19-20]

There are many well-known classes of organic photoswitches, including azobenzenes,[21] stilbenes,[22] diarylethenes,[23] spyropyrans,[24] fulgides,[25] and indigos.[6, 26] Diarylethenes (DAEs) have attracted broad interest due to their thermal stability and fatigue resistance,[27] which make them desirable photoswitchable building blocks for applications requiring thermal and chemical stability of both switch states and the ability to reverse through many cycles, as required for optical memory storage.[23] DAEs switch through reversible photoinduced cyclization and cycloreversion reactions upon exposure to UV and visible light, respectively.[27] Diaryl perfluorocyclopentene, in particular, is a common DAE switching motif, as the core cyclopentene ring eliminates the possibility for competing E/Z isomerization pathways.[27-28] The chemical structures of the pendant aryl groups

that form a nascent C-C bond through cyclization plays an important role in determining switch photoreactivity; these groups are commonly a modified thienyl or benzo[*b*]thienyl group bound to the ethene bridge via the β carbon (relative to S). Prior reports have demonstrated that the electron withdrawing or donating character of these groups impact the quantum yield (efficiency) for cycloreversion as well as the fatigue resistance for switching.[29-33] Whereas DAE cyclization is known to occur rapidly and with high efficiency, the dynamics and quantum yield for cycloreversion is controlled by branched (reactive vs. nonreactive) deactivation from the excited state of the cyclized structure.[34-37] Multiple reports have also detailed how cycloreversion yields can be manipulated through multiphoton excitation to states that access different deactivation pathways,[38-41] thereby presenting an additional, photonic handle for manipulating material properties.

Previous work from our labs extended the understanding of structure-response behaviors of DAEs by examining differences in the photoinduced cycloreversion of photoswitches between switches with different 'core' motifs bridging the pendant aryl groups.[42] Different core motifs studied included thienothiophene (TT), 1,1,2,2,3,3-hexafluorinatedcyclopentene, and 1H-pyrrole-2,5-dione. Photophysical and photochemical studies conducted with ultrafast transient absorption spectroscopy revealed that switching dynamics of the more rigid TT- and pyrrole-dione switches occurred three times faster than those of the cyclopentene switch. Temperature-dependent kinetics revealed that the excited-state potential-energy surfaces for the rigid-core structures are shallower overall than that of the structurally more flexible cyclopentene core.[36] Importantly, the structure of the core group did not impact the cycloreversion quantum yield for these switches, which arises from branched reactive and nonreactive deactivation that are both controlled by the relative topography of the excited-state potential-energy surface(s). In contrast changes to the pendant

groups impacted both the excited-state deactivation rate and cycloreversion quantum yield, with the differences attributable to the impact of the electron withdrawing/donating nature of the pendant group, similar to what has been found previous with other DAE derivatives.[30-31]

Understanding how structure impacts photochemical dynamics is critical to considering the integration of switches within more complex material architectures – such as switchable π-conjugated polymers,[19-20] polymeric ionic liquids,[43] or metal-organic frameworks[44-45] – in order to use light to control each system's properties. Nie *et. al.* found that changing the size of the anion in their polymeric ionic liquid altered the photostationary state of the DAE moiety, with larger anions increasing the mole fraction of the closed form of the switch, suggesting an impact on cyclization efficiency.[43] Peters and Tovar inserted thieno[3,4-*b*]thiophene (TT) core switches within an extended π-conjugation polymer by linking the TT core of the switch within the pi-conjugated backbone.[20] An earlier design for switchable pi-conjugated polymers linked switchable units via the pendant rings;[17, 46-51] a cross-conjugated design promises the separation of the cyclization/cycloreversion efficiencies from polymer or oligomer conformation or microstructure that is known to impact pendant-linked polymers. Yet, Peters and Tovar found that cross-conjugation of thienyl and phenyl groups to the TT core tends to inhibit cyclization of TT switches. Quantum-chemical calculations of the frontier molecular orbitals revealed that the cross conjugation to the TT core pulls the LUMO towards the π-conjugated backbone and away from the reactive carbon atoms on the pendant rings. Differences in energies of potentially reactive vs. nonreactive orbitals (and therefore reactive and nonreactive electronic states) between different cross-conjugated TT structures provided a basic understanding of why switching behavior was shut down for some of these structures.[20] Adams and Tovar expanded on this work to show that

the propensity to cyclize could be manipulated by introducing steric interactions that diminish cross-conjugated electronic coupling.[19]

These prior studies leave open questions about how the photoresponses of TT systems are altered by cross-conjugation. Here we provide a systematic study on the impacts of cross conjugation on TT photoreactivity using ultrafast and microsecond transient absorption spectroscopies to interrogate the evolution of excited switches and metastable photoproducts and states populated through photoexcitation. Utilizing a series of TT core switches with different cross-conjugated backbones, we reveal the differences in relaxation dynamics that occur in reactive vs. non-reactive cross-conjugated structures and how the balance of reactive and nonreactive deactivation pathways could be controlled structurally in cross-conjugated switch structures.

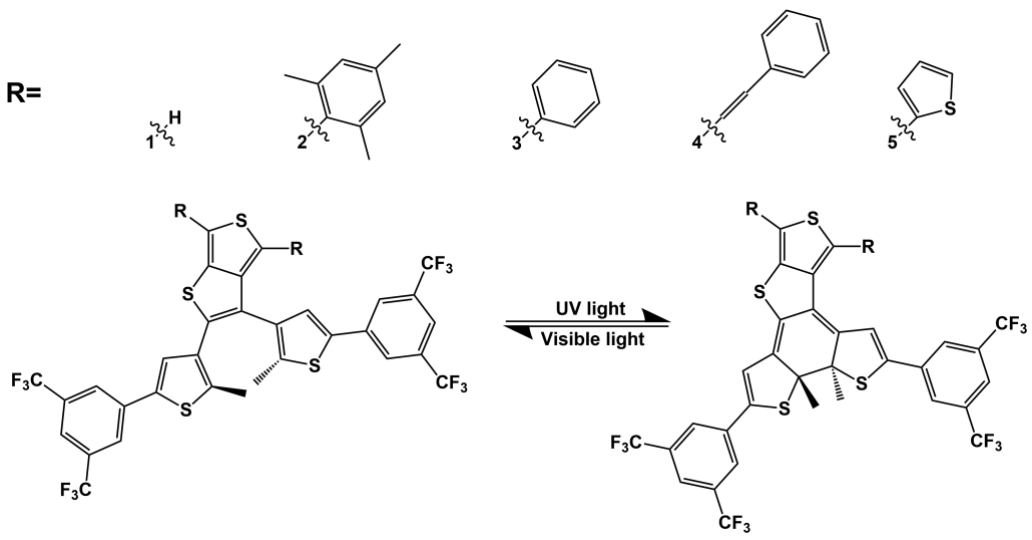

Scheme 1. Reversible photoswitching between open and cyclized structural isomers of diaryl thieno[3,4-b]thiophene. Structures studied here differ according to the identity of the R group. **1. TT2**, **2. TT2-mes**, **3. TT2-Ph**, **4. TT2-APh**, and **5. TT2-Th**. Full compound names are given in the Experimental Methods section.

Experimental Methods

Sample Preparation and Handling

Structures of the switches considered in this work are shown in Scheme 1 and include 2,3-bis(5-(3,5-bis(trifluoromethyl)phenyl)-2-methylthiophen-3-yl)thieno[3,4-b]thiophene (**TT2**),[17] 2,3-bis(5-(3,5-bis(trifluoromethyl)phenyl)-2-methylthiophen-3-yl)-4,6-diphenylthieno[3,4-b]thiophene (**TT2-Ph**),[17] 2,3-bis(5-(3,5-bis(trifluoromethyl)phenyl)-2-methylthiophen-3-yl)-4,6-di(thiophen-2-yl)thieno[3,4-b]thiophene (**TT2-Th**), 2,3-bis(5-(3,5-bis(trifluoromethyl)phenyl)-2-methylthiophen-3-yl)-4,6-bis(phenylethynyl)thieno[3,4-b]thiophene (**TT2-APh**),[19] and 2,3-bis(5-(3,5-bis(trifluoromethyl)phenyl)-2-methylthiophen-3-yl)-4,6-dimesitylthieno[3,4-b]thiophene (**TT2-mes**).[19] **TT2** and **TT2-Ph** were synthesized and purified as described by Peters and Tovar.[20] The synthesis and purification of **TT2-mes** and **TT2-APh** has been described by Adams and Tovar.[19] The synthesis and purification of **TT2-Th** were performed as described in the Supporting Information (pages S2-S5, with ^{1}H and ^{13}C NMR spectra presented in Figures S1 and S2, respectively). Solutions of each switch were prepared in acetonitrile at concentrations ranging 40-600 μM. **TT2-mes** was prepared at 40 μM due to limited availability. Microsecond measurements were performed with concentrations at the high end of this range due to a lower sensitivity with the microsecond TA setup. Samples were stored in the dark to prevent unwanted photoinduced cyclization and degradation from exposure to ambient lighting. For laser measurements, sample solutions were stored in a round-bottom flask reservoir and circulated through a fused-silica flow cell (variable pathlength cell from Harrick Scientific Products or 1-mm quartz flow cell from Spectrocell) to prevent the buildup of cyclized photoproduct in the beam path during transient absorption measurements. The sample reservoir was irradiated with a general-purpose LED lamp to revert any cyclized products generated with UV excitation for TA measurements to the uncyclized/open photoreactant structures (Scheme 1). The Harrick cell optical pathlength was

adjusted from 0.5 mm or 0.95 mm, depending on the optical density of the open structure at 266 nm. Due to limited sample availability, experiments with **TT2-mes** were conducted with solutions in a stirred 2 mm quartz cuvette instead of the flow cell; in order to collect data before any possible accumulation of cyclized photoproduct within the cuvette, the number of time delays sampled past 5 ps was limited.

Transient Absorption Spectroscopy

Laser pulses for ultrafast and microsecond experiments were generated using a regeneratively amplified Ti:sapphire laser (Coherent Legend Elite, 1 kHz repetition rate, 35 fs pulse duration, 3.5 mJ per pulse, 800 nm peak wavelength). 266 nm pump pulses were generated for sample excitation using a doubling+mixing scheme: a portion of the 800 nm fundamental was converted to 400 nm by second harmonic generation in a 200 μm thick type I BBO crystal; the second harmonic was then mixed with 800 nm fundamental in a 150 μm type II BBO crystal to generate 266 nm pulses.[52] Broadband probe pulses were obtained by focusing <1 μJ of the 800 nm fundamental into a 2-mm-thick sapphire or a 3-mm-thick calcium fluoride plate, to drive white-light generation. TA measurements were performed with the pump and probe polarizations at "magic angle" in order to remove time-dependence due to orientational diffusion. Magic angle was achieved by using a wire-grid polarizer aligned for transmission at 54.7° relative to the pump polarization as the last optic in the probe beam path before the sample. The pump beam-path included parallel reflections on to and off of a hollow corner-cube mirror mounted on a motorized translation stage (Newport); the pump-probe time delay was controlled by adjusting the stage position.

Detection of transient absorption signal in the visible and the near-IR was performed simultaneously. The probe beam was collimated after the sample and a neutral density filter was

used to split the broadband continuum into 2 portions, each of which was sent to a different detector for visible or near-IR sensing. Visible light (450-750 nm) was detected by dispersing the continuum with a spectrograph (Acton-2360) onto a CCD camera (Pixis-100BR, Princeton Instruments), as described previously.[52] Near-IR detection used a prism spectrograph to disperse infrared light (700-1400 nm) onto an InGaAs detector (Hamamatsu G11608) configured in a manner similar to the system described by Schmidhammer, *et. al*.[53] A combination of 800 nm and 830 nm long-pass filters positioned in front of the InGaAs array was required to cut down the light intensity below 850 nm, including scattered laser fundamental. Customized Labview programs were used acquire data from both detectors. NIR detection was laser triggered with chopper phases and light intensities obtained on every trigger in order to calculate a transient absorption spectrum on a shot-to-shot basis. Time delays were scanned using the visible TAS acquisition program, which interfaced directly with translation stage and CCD camera. NIR TA spectra were assigned to time delays by digitizing the position encoding of the translation stage on the fly. The prism spectrograph + InGaAs detector pair was calibrated using the NIR lines from mercury pen and halogen lamps.

Global target analysis of TA spectra was performed using Python scripts. Global fits of data were based on 3 and 4 component sequential kinetics models, Equation 1, fit to the data using the Levenberg-Marquardt method for non-linear least squares fitting.[54] The kinetics models were convolved with a normalized gaussian instrument response function.

$$A \underset{k_1}{\rightarrow} B \underset{k_2}{\rightarrow} C \qquad \text{Equation 1a}$$

$$A \underset{k_1}{\rightarrow} B \underset{k_2}{\rightarrow} C \underset{k_3}{\rightarrow} D \qquad \text{Equation 1b}$$

For the fits presented in this paper, species A often accounted for nonlinear, coherent artifacts produced in the signal around time zero. These artifacts are a product of interactions that occur when the pump and probe pulses are overlapped in time as they pass through the sample.[55] Hence, species A produced by the fits generally has a very short lifetime, less than 200 fs in all cases except **TT2** where this lifetime is 220 fs, and is regarded as having no physical meaning to explain the dynamics observed in the sample. This attribution is justified by the effective time-resolution or temporal instrument response (~200 fs), that we have previously characterized for this experimental set-up for UV pump/WL probe experiments by cross-correlation.[56]

Finally, we note that the species associated difference spectra (SADS) obtained by GA are formally the same as evolution associated difference spectra (EADS). We chose to analyze the data in this way, rather than using decay associated difference spectra (DADS) obtained from a multiexponential fit, because we believe that it provides the best insights for understanding photochemical dynamics when there are cascading relaxation processes.

Microsecond TA Spectroscopy

Microsecond-resolved TA spectra were obtained using a xenon flash lamp (Hamamatsu L13651-11) running at 250 Hz and controlled by a BNC-555 Delay Generator as the probe light source. For these measurements, the CCD was triggered to sample at 500 Hz. The 1 kHz pump beam was chopped mechanically at both 500 and 125 Hz, resulting in an on-on-off-off pump sequence at 125 Hz that is synchronized with the probe on-off-on-off sequence that results when the flash lamp is triggered at 250 Hz. To access microsecond delays, a separate channel of the amplifier's signal delay generator (SDG Elite) was used to trigger a BNC-555 that in turn was used to trigger the flash lamp. This channel's delay could be controlled and adjusted with a Labview-based data acquisition program, allowing automated scans through delays for data collection. All

other components of the set-up were the same as the ultrafast TA set-up, allowing for collection of microsecond data in the same way, but requiring twice the runtime for averaging a similar number of spectra.

Results

Steady-state characterization

UV-Vis absorption spectra of **TT2** and its analogues (Scheme 1) in acetonitrile solutions before (black) and after (red) irradiation with 254 nm light from a handheld UV lamp, are plotted in Figure 1 (a-e). Samples were exposed to UV for between 2-15 min to guarantee formation of photoproduct or lack thereof. These spectra have been published and discussed in detail elsewhere,[19-20] but are included here to establish the structure-dependent sensitivity of photoswitching that we interrogate using transient absorption spectroscopy in this work. As seen in Figure 1(a), **TT2** exhibits an absorption peak at 290 nm with a shoulder at ~310 nm. In contrast, its corresponding cyclized structure exhibits new features peaking at 620 nm and 390 nm.[23] These features are similar to those of open and cyclized diarylethene structures reported previously.[30, 57-58] The spectral differences for cyclized vs. "open-ring" structures is due to an increase in delocalized π-conjugation in the cyclized state.[59] Uncyclized (open-ring) diarylethene analogs can exist in both parallel and antiparallel conformations (i.e. with methyl groups on the opposite vs. the same side of the plane defined by the ethene bond, respectively) due to "free" rotation about the bond linking the pendant aryl groups to the core unit. This rotation and associated non-planarity in combination with the aromaticity of the aryl rings limits π delocalization across the switch structure. However, the molecule loses two pi electrons during sigma bond formation, thereby destroying the aromaticity of the constituent rings, and becomes locked in a more planar

configuration upon cyclization, which in combination facilitate π delocalization across the entire molecule (see Scheme 1).

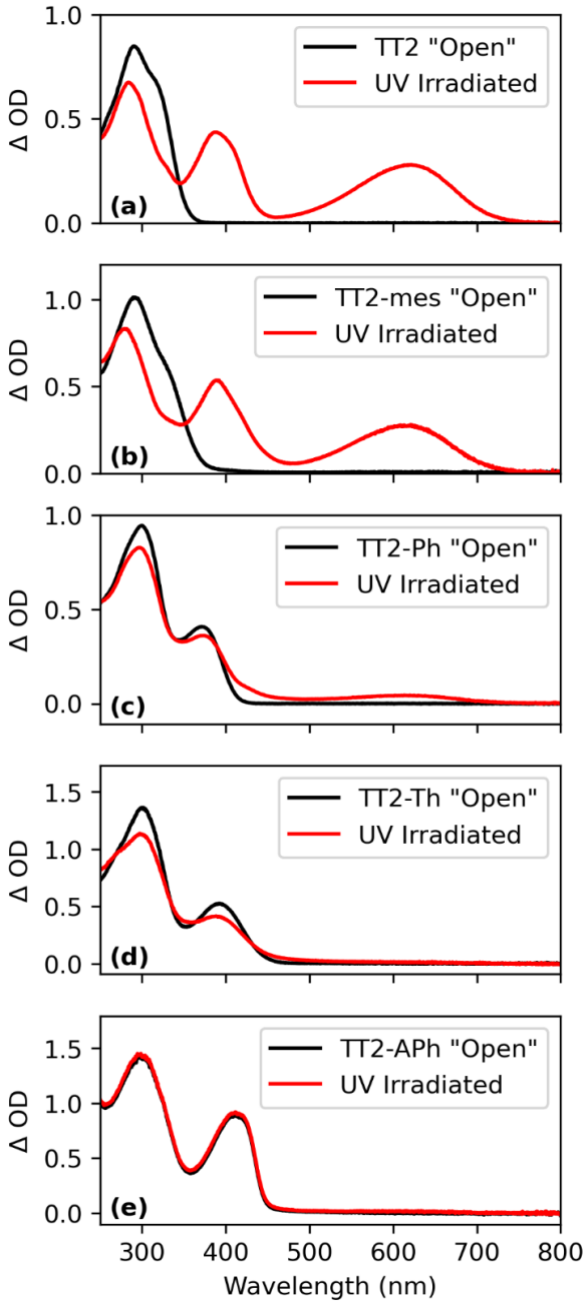

Figure 1. Steady-state UV-Vis absorption spectra of solutions of **TT2** and its cross-conjugated analogues in acetonitrile before (black) and after (red) UV irradiation. **(a) TT2**, **(b) TT2-mes**, **(c) TT2-Ph**, **(d) TT2-Th**, and **(e) TT2-APh**.

Two significant trends are observed as π-conjugated ("non-pendant") aryl substituents are appended to the **TT2** core at the 4,6 positions that are correlated with the degree of pi-conjugation across this conjugated "backbone." Firstly, the extent of photoswitching is inhibited, as is clear from the observed decrease in the magnitude of the 620 nm absorption feature observed with UV irradiation (Figure 1): whereas cyclization remains highly favorable for **TT2-mes** (relative to **TT2** itself), the cyclization yield is qualitatively much lower for **TT2-Ph** and is virtually zero for **TT2-Th** and **TT2-APh**. Secondly, the absorption shoulder observed for **TT2** at 310 nm (Figure 1(a)) progressively redshifts as pi-conjugation between the TT 'core' and cross-linked backbone is enhanced: for **TT2-mes** (Figure 1(b)), this feature still appears as a shoulder to the more intense absorption feature at 290 nm, but peaks distinctly at 370 nm for **TT2-Ph** (Figure 1(c)) and further redshifts to 390 nm and 410 nm for **TT2-Th** (Figure 1(d)) and **TT2-APh** (Figure 1(e)), respectively. In contrast, the highest energy peak (290 nm) observed with open switches and the positions of features observed for cyclized structures (e.g. 620 nm) shift only weakly across this series of structures. The shifts of all peak positions in the UV-Vis absorption spectra are summarized with Figure 2.

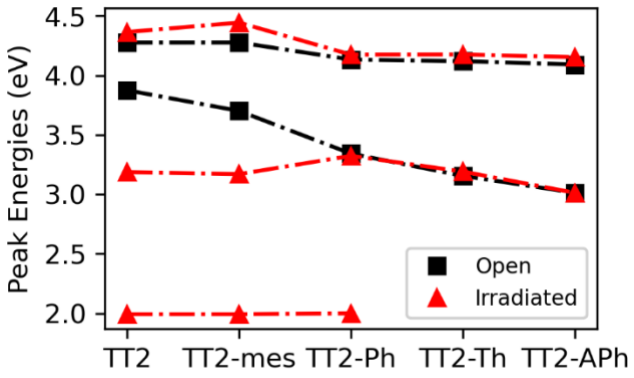

Figure 2. Peak energies for steady-state spectra of **TT2** and its cross conjugated analogues before (black) and after (red) irradiation with UV light.

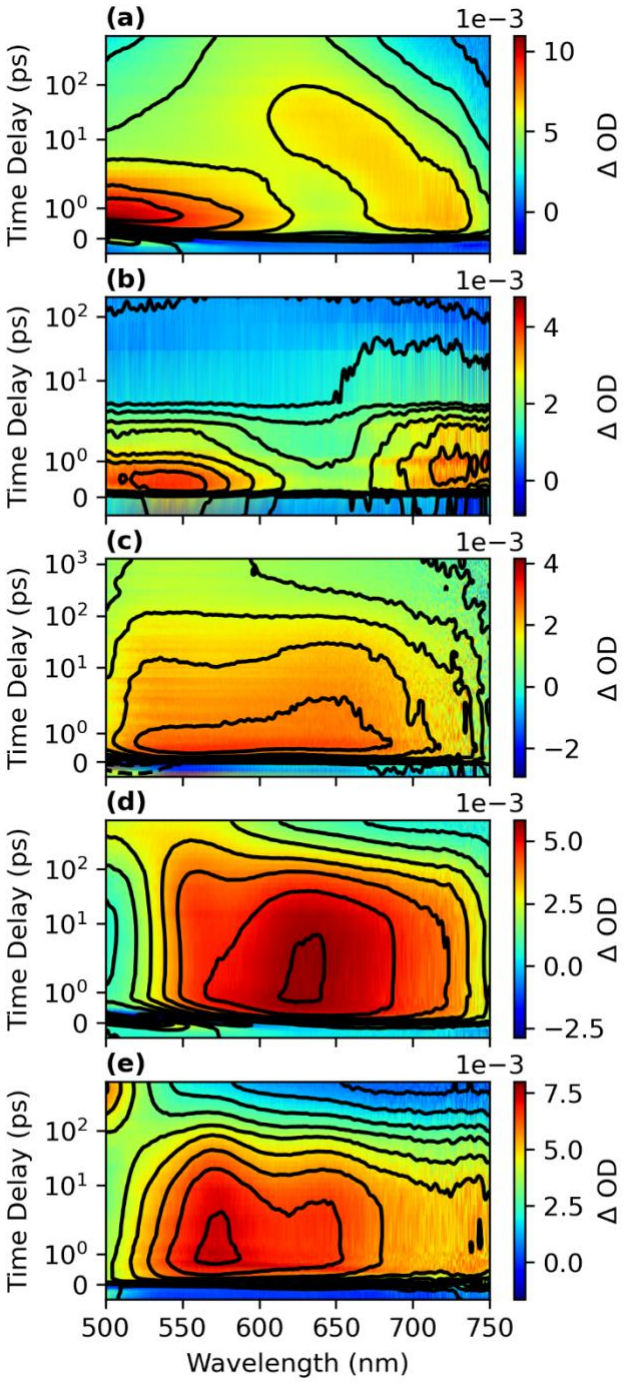

Figure 3. Ultrafast transient absorption spectra collected with **TT2** and its cross-conjugated analogues in acetonitrile. All TA spectra collected were obtained using 266-nm excitation pulses. **(a) TT2**, **(b) TT2-mes**, **(c) TT2-Ph**, **(d) TT2-Th**, and **(e) TT2-APh**.

Ultrafast characterization of excited-state dynamics of **TT2** and its cross-conjugated analogues

Ultrafast Photoinduced Dynamics of TT2 and TT2-mes. Figure 3 presents a false-color contour plot of ultrafast transient absorption data obtained with 266-nm excitation for all TT-core switches studied in this work; the same data is presented as waterfall plots in Figure S3. Additional data collected with near IR probe continua and 400 nm excitation pulses are presented in Figures S4-S6 and Figures S7-S9, respectively. Figure 3(a) presents results for **TT2**. Immediately following excitation, **TT2** exhibits two photoinduced absorption features centered at ~540 nm and ~750 nm, where the latter extends into the NIR, as shown in Figure S4. These features decay within roughly 1.5 ps, interconverting to a new broad absorption feature centered at 670 nm. The latter persists for the remaining time delays (up to 1 ns), but blue shifts to 620 nm on a timescale of roughly 100 ps.

Figure 4(a) presents the species associated difference spectra (SADS) obtained from global target analysis of **TT2** TAS data using a 4-component sequential kinetic model summarized by Equation 1b; the lifetimes of each SADS are summarized in Table 1, while fits to time-dependent signals at representative wavelengths are presented in Figure 5(a). SADS 1 is very short lived and is ascribed to a coherent spectral artifact that arises at time zero and does not have physical meaning for the dynamics of **TT2**. SADS 2 represents the absorption features captured for photoexcited **TT2** immediately after excitation. These features decay rapidly, on a timescale of 1.42 ps (Table 1), to SADS 3, which corresponds with the 670 nm absorption feature seen in the **TT2** data. SADS 3 persists for much longer than SADS 2 with a lifetime of 110 ps. SADS 4 features a broad visible absorbance centered on 620 nm. The interconversion of SADS 3 to SADS 4 is representative of the blue shift observed in the TA spectra shown in Figure 3(a). Notably,

SADS 4 is in good agreement with the spectrum of the photoproduct observed with steady-state absorption spectroscopy (Figure 1(a)).

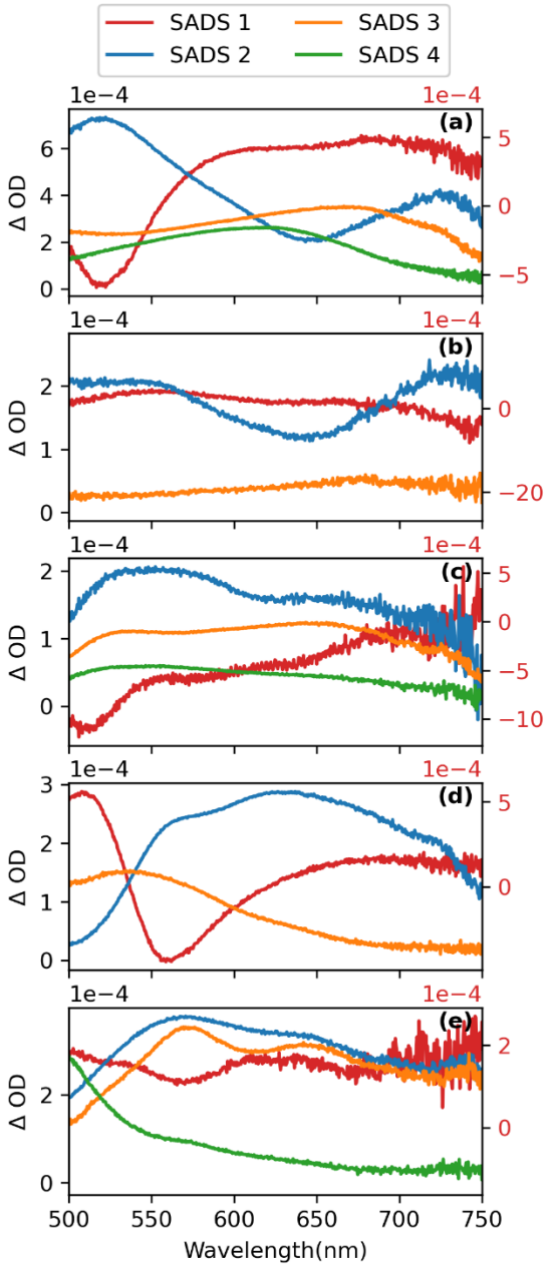

Figure 4. Species associated difference spectra (SADS) obtained by fitting TAS data collected with **TT2** and its cross-conjugated analogues using global analysis with sequential kinetics models presented in Equations 1. SADS 1 (red) is plotted on a separate scale on the right. **(a) TT2**, **(b) TT2-mes**, **(c) TT2-Ph**, **(d) TT2-Th**, and **(e) TT2-APh**.

Table 1. Lifetimes (in picoseconds) associated with SADS (Figure 4) obtained from global fitting of TAS data obtained with **TT2** and its cross-conjugated analogues (Figure 3).

Lifetime (ps)	***TT2***	***TT2-mes***	***TT2-Ph***	***TT2-Th***	***TT2-APh***
τ_1	0.22±0.01	0.089±0.008	0.01±0.06	0.142±0.004	0.162±0.007
τ_2	1.42±0.08	2.89±0.08	0.73±0.06	184±6	5.03±1.5
τ_3	109±8	-	91±3	-	133±4

TAS data collected with **TT2-mes** is presented in Figure 3(b) with SADS from global analysis presented in Figure 4(b) and fitted cuts at representative wavelengths in Figure 5(b). The initial photoinduced spectrum for **TT2-mes** is similar to that observed for **TT2**, with photoinduced absorption bands at 540 and 750 nm. Both features decay rapidly, within ~3 ps, to a broad absorption feature that is centered at 680 nm that lives to 200 ps. As noted in the experimental section, time delays were sampled sparsely for TAS measurements with **TT2-mes** due to a limited sample solution and concern for the possible buildup of the cyclized photoproduct that absorbs at the excitation wavelength during the course of a long TAS measurement. The SADS of **TT2-mes** show very similar features as the SADS obtained from the fit of **TT2** TAS data. Because the data collected with **TT2-mes** does not span the full length of delays used with **TT2** TAS data, the former is fit with a 3-component sequential kinetic model. SADS 2 and 3 for **TT2-mes** are similar to SADS 2 and 3 obtained from **TT2** data, with both exhibiting two initial absorption features centered at 540 and 750 nm, that decay within a few ps to a broad absorption band centered around 670 nm.

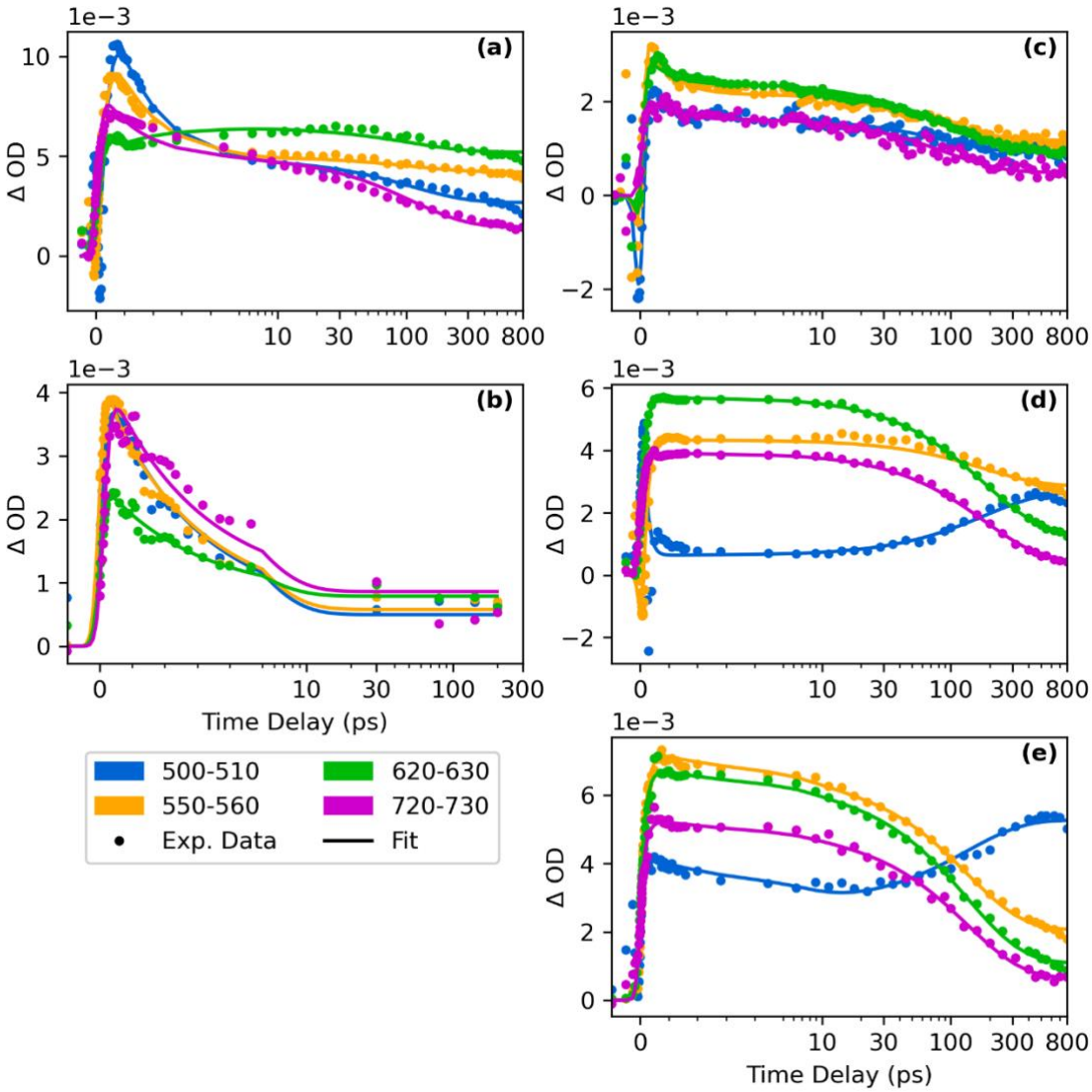

Figure 5. Time-dependence of TA spectra at selected wavelengths (dots) plotted with fit lines obtained using global analysis. **(a) TT2**, **(b) TT2-mes**, **(c) TT2-Ph**, **(d) TT2-Th**, and **(e) TT2-APh**.

Ultrafast Photoinduced Dynamics of TT2-Th and TT2-APh. Figures 3(d), 4(d), and 5(d) present TAS data, SADS, and fitted time-dependent traces at select probe wavelengths for **TT2-Th**, which exhibits very different spectral dynamics compared to **TT2** and **TT2-mes**. Upon excitation, a broad absorption feature appears that extends throughout the detection window in the visible and peaks around 630 nm. This feature decays on a much longer timescale than the

photoinduced features observed in SADS 2 for **TT2** and **TT2-mes**, with a lifetime of ~180 ps. The initial feature decays with the appearance of a peak at bluer wavelengths, centered around 540 nm, that persists up to 1 ns. While this feature could potentially arise from a photoproduct, the lack of any representative photoproduct absorbance in steady-state data suggests that this feature is associated with a state populated as part of a nonreactive deactivation pathway. We discuss the fate of this photoinduced absorption in connection with microsecond TAS experiments further below.

TT2-APh data, represented with Figures 3(e), 4(e) and 5(e), shows similar excited-state spectral dynamics as those observed for **TT2-Th**. An initial broad absorption peaking around 560 nm decays after ~130 ps into a long-lived absorption peaked near the blue edge of the spectral window of the probe. The similarities between SADS 2 of **TT2-Th** and **TT2-APh** and SADS 3 of **TT2-Th** and SADS 4 of **TT2-APh** suggest similar nonreactive relaxation pathways for both molecules. The lack of photoproduct generated with steady-state UV irradiation for both molecules reinforces this hypothesis. The extra component in **TT2-APh**, SADS 3, is believed to be the result of vibrational relaxation of the initial excited state, captured by SADS 2. SADS 3 closely mirrors SADS 2 in overall shape but has sharper peaks and lower intensities. The 5-ps lifetime between SADS 2 and 3 also suggests that rapid vibrational relaxation post excitation is responsible for the change between SADS 2 and 3. Neither **TT2-Th** nor **TT2-APh** show significant new features in the NIR, as shown in Figures S5 and S6.

Notably, all of the TA measurements described above were conducted with photoexcitation at 266 nm, above the highest energy features appearing in the steady-state absorption spectra shown in Figure 1. TA experiments were repeated for **TT2-Th** and **TT2-APh** using 400 nm pump pulses, which are resonant with the lowest energy feature that shifts with modifications in structure

of the switches' cross-conjugated "backbone." The resulting spectra and fits are presented in Figures S7-S9. Despite the lower excitation energy, the resulting TA data showed similar spectral signals and time evolution as observed with excitation at 266 nm. Fitting the 400 nm data to the same parameters obtained with 266-nm excitation produced reasonable fit results (Figures S8-S9), suggesting that the same dynamics are responsible for the signals seen in both datasets.

Ultrafast Photoinduced Dynamics of TT2-Ph. The excited-state spectral dynamics of **TT2-Ph**, presented in Figure 3(c), are distinct relative to all other **TT2** analogues. Upon excitation, there is a broad absorption feature that rises with two overlapping bands, one centered at 550 nm and the other around 670 nm. A broad signal persists through the 1.5-ns probed time range, but the intensities of the two bands that make up the signal change with time. Immediately after excitation, the band centered at 550 nm has greater intensity than the band at 670 nm. Within 1 ps, the intensity of the 550-nm band decreases and the 670 nm band has the greater intensity. The balance shifts once more as the time delays progress past 100 ps (the 670-nm band decreases in intensity compared to the signal at 550 nm). These signal changes are reflected in the SADS for **TT2-Ph** plotted in Figure 4(c) and the time-dependent cuts at select wavelengths plotted in Figure 5(c). The final photoinduced absorption feature observed for **TT2-Ph** is similar to those observed for the non-cyclizing **TT2-Th** and **APh**. Nevertheless, steady-state data presented in Figure 1(c) confirms that **TT2-Ph** does photocyclize upon UV exposure. These observations suggest that more than one deactivation pathway is active for **TT2-Ph**.

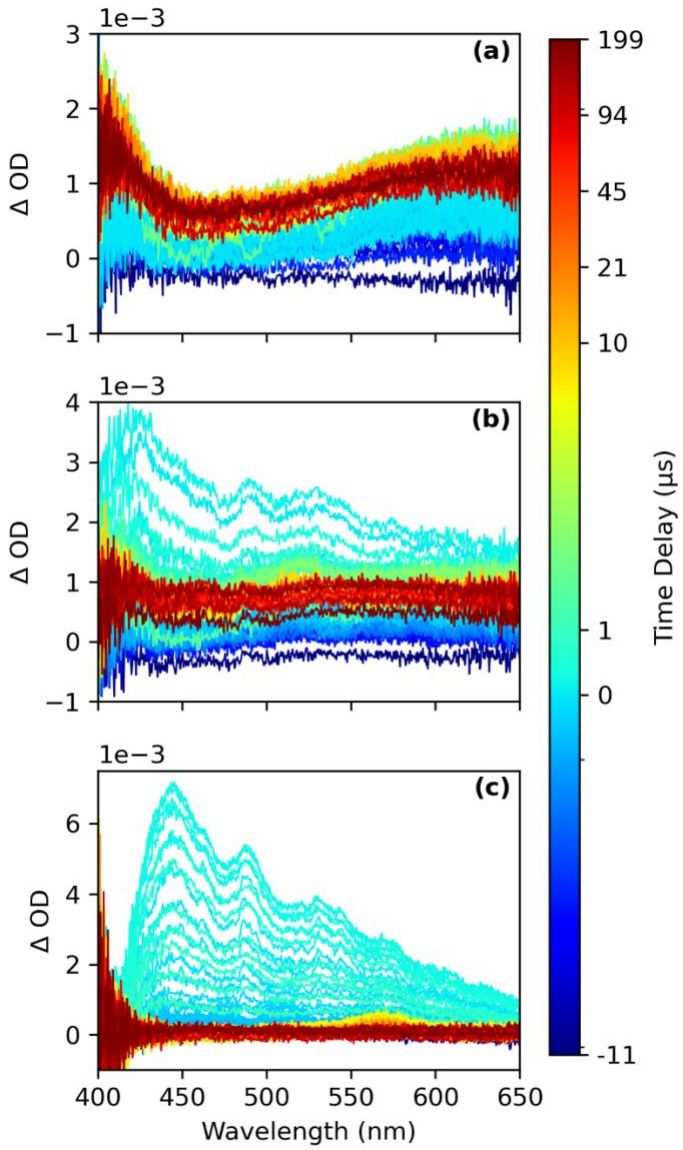

Figure 6. Microsecond transient absorption data obtained with selected **TT2** structures. Data was collected in acetonitrile with a 266 nm pump. **(a) TT2**, **(b) TT2-Ph**, and **(c) TT2-Th**.

Metastable states interrogated by Microsecond TAS

The absorption features observed for **TT2** and **TT2-Th** at the latest delays probed in ultrafast TAS experiments warrant further investigation to ascertain whether they represent cyclized photoproducts or rather an intermediate or metastable photophysical state associated with each structure. Microsecond TA experiments were used to bridge the gap between ultrafast transient absorption and steady-state irradiation experiments shown in Figures 3 and 1, respectively. Figures 6(a-c) present microsecond TAS data obtained with **TT2**, **TT2-Th**, and **TT2-Ph**, while Figure 7 presents the time dependence of the average signal in the probe wavelength range of 420-430 nm for each data set. The microsecond TAS data for **TT2**, Figure 6(a), shows photoinduced absorption that matches the spectrum of the cyclized photoproduct (Figure 1(a)), represented by the 620 nm absorption feature and a more intense feature below 450 nm. These features appear within the resolution of the microsecond TAS experiment and persist for 100s of microseconds, confirming assignment of the spectral dynamics observed in ultrafast measurements to cyclization.

Conversely, microsecond data for **TT2-Th**, Figure 6(b), exhibits a photoinduced absorption feature that is reminiscent of the photoinduced absorption observed at the latest delays probed in our ultrafast TAS measurements. This feature decays within 1 microsecond, with no further signals observed on microsecond timescales. This signal is reminiscent in spectral shape and lifetime to triplet absorption features that have been observed for conjugated thiophene oligomers.[60]

Microsecond TAS data for **TT2-Ph**, presented in Figure 6(c), has features common to data collected for both **TT2** and **TT2-Th**: at very short time delays, the photoinduced absorption spectrum is similar to that observed for **TT2-Th**, with a peak at 420 nm. This feature decays for

both **TT2-Th** and **TT2-Ph** in around 1 μs; however, unlike **TT2-Th**, another long-lived absorption feature persists through (and beyond) 200 microseconds. This final feature appears as a broad absorption feature, spanning the entire probe range, and is similar to the absorption band observed by steady-state absorption after UV exposure of **TT2-Ph** solutions. **TT2-Ph** shows much lower efficiency for switching than **TT2**, such that the photoproduct absorption features are expected to appear at much smaller optical densities in microsecond data for the former. The observation of spectral kinetics common to **TT2-Th** and **TT2** in the microsecond data for **TT2-Ph** suggests that this structure exhibits competing photoinduced relaxation pathways: reactive and nonreactive.

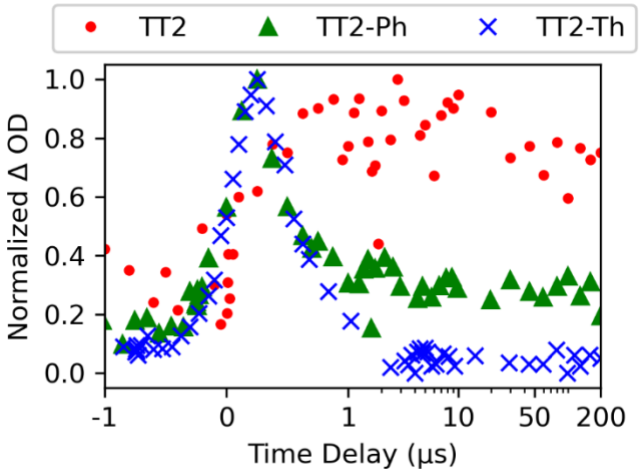

Figure 7. Averaged intensity in the probe wavelength range of 420-430 nm from microsecond TA data obtained with **TT2**, **TT2-Ph** and **TT2-Th**. Optical densities are normalized to the maximum value obtained with each sample in this range.

Discussion

Based on the results of TA experiments conducted with **TT2** analogues on both ultrafast and microsecond timescales, we propose two distinct pathways for deactivation following UV excitation: The first, faithfully exhibited by **TT2** and **TT2-mes**, involves a reactive deactivation

via rapid nonadiabatic photocyclization to produce a vibrationally hot photoproduct in its electronic ground state; this step is captured by the spectral evolution between SADS 2 and SADS 3 for **TT2** in Figures 3(a) and 4(a). The cyclized photoproduct subsequently thermalizes on a slower timescale, as captured by the progression from SADS 3 to SADS 4 for **TT2**; the spectral blue-shift of the photoproduct absorption observed by TAS is consistent with expected changes in the Franck-Condon profile of this transition with vibrational cooling (i.e., disappearance of hot-band spectral intensity at longer wavelengths). These dynamics are associated with the canonical 6pi electrocyclization of diarylethenes, with timescales similar to those observed for related diarylethene photoswitches.[34] The initial rapid relaxation of **TT2-mes** observed by ultrafast TAS, which involves SADS that are similar to those obtained for **TT2** as well as the steady-state photochemical data presented in Figure 1(b), support that this cross-conjugated structure also exhibits reactive photochemical dynamics. This photochemical pathway is summarized by the solid green arrows in the energy-level diagram presented in Figure 8.

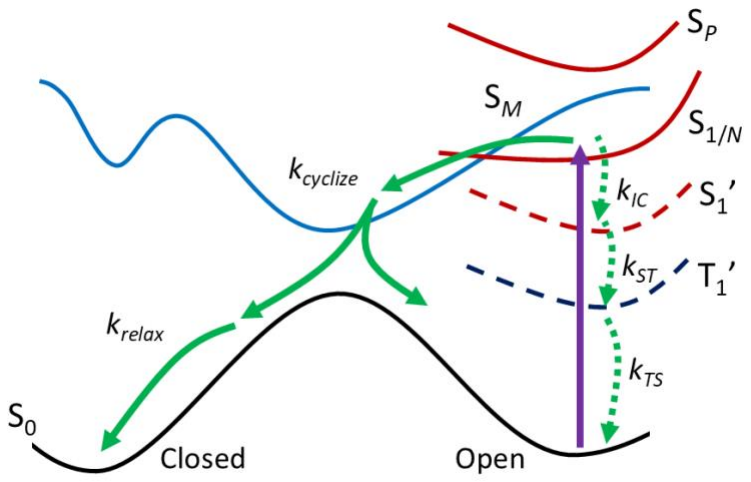

Figure 8. Energy-level diagram demonstrating the competing relaxation pathways observed for the cross-conjugated TT switches studied in the present work.

In contrast, **TT2-Th** and **TT2-APh** faithfully exhibit spectral dynamics associated with a different deactivation pathway, whereby the photoprepared excited state in each molecule decays photophysically (i.e. nonreactively) with a dominant contribution from intersystem crossing to the triplet manifold. This proposed mechanism is supported by the comparatively longer excited-state lifetime of the photoexcited switch in both **TT2-Th** and **TT2-APh** vs. **TT2** and **TT2-mes** (i.e., ~100 ps vs. a few ps), as well as the spectral shape and decay rate associated with the absorption feature observed for **TT2-Th** on sub-microsecond timescales. Indeed, the triplet absorption spectra of conjugated oligomers have similar absorption signals to what we observe by TAS with **TT2-Th** and **APh**:[60-61] particularly, Rentsch, *et. al.* measured the triplet absorption spectrum of α-terthiophene, which strongly resembles the microsecond TA spectrum of **TT2-Th** presented in Figure 6(b).[60] Both spectra exhibit a peak around 450 nm with a long tail extending towards the red and appear within 100s of ps after excitation. The similarity in the triplet spectra is attributed to the strong conjugation of the thienothiophene core within a Th-TT-Th backbone, such that the chromophore in **TT2-Th** is dominated by the spectral properties of the backbone. The similarly rapid photophysical deactivation rates of **TT2-Th** and α-terthiophene could potentially be attributed, qualitatively, to the influence of sulfur on the spin-orbital coupling and ISC rate constant (i.e., "heavy atom effect"). This photophysical pathway is summarized with the dotted green arrows in the energy-level diagram presented in Figure 8.

Previously, Peters *et. al.* used DFT calculations to compare the electron density associated with the HOMO and LUMO orbitals in phenyl cross-conjugated TT structures.[20] They observed a shift in electron density of the LUMO as the pendant group changed. Pendant groups with stronger π-conjugation were able to better maintain photoreactivity when the TT core was cross-conjugated

with benzene.[20] Photoreactive switches were observed to maintain electron density in the LUMO near the reactive C sites on the pendant rings whereas nonreactive switches had greater density along the backbone. More recent work performed by Adams *et. al.* performed similar calculations but varied only the cross-conjugated backbone.[19] Their frontier molecular orbital calculations demonstrate similar results to Peters *et. al.,* with shifts in LUMO density to or away from the backbone depending on the strength of π-conjugation between the TT core and cross-conjugating substituents.

The changes in electron density observed in these previous studies are consistent with the redshift in the lowest-energy absorption feature observed for the (open) switch states (Figures 1 and 2), due to increased pi-delocalization along the backbone of the switch, and is believed to be responsible for the loss of switching behavior with cross-conjugation. Our data further supports this interpretation by providing insights on the photophysical fate of excited switches with different degrees of pi-delocalization within the cross-conjugated backbone: as the LUMO character is distributed across the core/backbone of cross-conjugated **TT2** switches, the excited-state dynamics are more dependent on the relaxation of backbone and therefore resemble deactivation dynamics of small conjugated oligomers. Interestingly, the highest-energy absorption feature (~290 nm) recorded for the **TT2** switch family does not shift significantly with modification to the cross-conjugated structure, suggesting that the initial excitation at 266 nm prepares a state that may have an LUMO electron density localized in the region of the switching motif. Rapid deactivation of the photoprepared state to a low-lying excited electronic state delocalized along the conjugated backbone is therefore responsible for the termination of switching with cross-conjugation in **TT2-Th** and **TT2-APh**.

TT2-Ph presents an interesting intermediate case: Figure 1(c) demonstrates the buildup of photoproduct upon irradiation with UV light, but the ultrafast TA spectra collected a few picoseconds after excitation resemble the TA signals observed with **TT2-Th**. Furthermore, the microsecond data obtained for **TT2-Ph** (Figure 6(c)) exhibits a photoinduced absorption feature on sub-microsecond timescales that is similar to what is observed for **TT2-Th**, but as this signal decays, **TT2-Ph** exhibits a long-lived absorption feature attributable to a cyclized photoproduct that is not observed with **TT2-Th**. Thus, in combination, Figures 1(c), 3(c), 4(c), 6(c) and 7 demonstrate that both pathways are active for **TT2-Ph**. Peters *et. al.* calculations with **TT2-Ph** showed that the LUMO and LUMO+1 orbitals for **TT2-Ph** are close in relative energy with a difference of ~0.1 eV between them using B3LYP/6-311G(d). Importantly, the LUMO is localized more on the pendant groups and TT core, reminiscent of the unsubstituted switching motif, but the LUMO+1 appears to be delocalized on the cross-conjugated backbone, which would be conducive to nonreactive deactivation. The close energy gap between these two orbitals, one showing electron density needed for the photochromic reaction and the other not, can explain why competitive relaxation dynamics can be observed in **TT2-Ph**, but not in any other switch examined in our work. For Peters *et. al.*, no other switch they studied had energy gaps between reactive and nonreactive unoccupied states as small as those of **TT2-Ph**.[20]

This duality can be further rationalized in part by the sterically perturbed pi stabilization along the conjugated backbone in **TT2-Ph** (relative to **TT2-Th** and **-Aph**) that would temper the withdrawal of electron density away from the reactive carbon sites in the excited state. The smaller shift of the lowest-energy absorption feature relative to **TT2** itself (compared to **TT2-Th** and **TT2-APh**) from ~3.7 to ~3.3 eV (Figures 1 and 2) is consistent with weaker withdrawal of electron density from the photochemically reactive carbon sites. The bimodal excited-state kinetics

observed in Figures 3(c) and 5(c) for **TT2-Ph** are seemingly associated with the disparate timescales for cyclization and nonreactive photophysical deactivation observed in **TT2**/**TT2-mes** vs. **TT2-Th**/**TT2-APh**. We anticipate that the rate of cyclization should further decrease with increased pi stabilization in the backbone of **TT2-Ph** vs. **TT2-mes**, such that the dynamics of cyclization could occur on comparable timescales as (and in parallel with) the nonreactive deactivation dynamics (ISC). Nonetheless, a rapid component of the excited-state deactivation for **TT2-Ph** occurs on timescales faster than what is observed for either **TT2** and **TT2-mes**. We therefore posit that switching of **TT2-Ph** may be more efficient prior to thermalization of excess energy in a low-lying excited state dominated by the properties of the cross-conjugated chain.

Conclusions

We have investigated the photochemical and photophysical impacts of cross-conjugating the core unit in a family of diaryl thienothiophene photoswitches. We find that the addition of a π-conjugated backbone onto TT switches impedes the photoreactivity of the core switching motif by introducing an alternative nonreactive deactivation pathway that is dominated by intersystem crossing to a triplet state. The strength of π conjugation through the TT core (as manifested through torsional strain and dihedral angle alteration along the carbon-carbon single bonds joining the arenes to the TT core) determines whether reactive or nonreactive deactivation prevail: when the switch structure has strong π conjugation across the cross-conjugated "backbone," as in **TT2-APh** and **TT2-Th**, the excited switch deactivates through a long-lived triplet state, similar to related conjugated oligomers, without cyclizing. With weaker π conjugation in the cross-conjugated backbone, cyclization dominates (e.g. **TT2-mes)** or can compete with nonreactive deactivation (as is the case for **TT2-Ph** which exhibits signatures of both deactivation pathways). These

mechanisms are consistent with expectations for electron withdrawal from the reactive sites of the core switching motif with increased π-interactions along the cross-conjugated backbone that should favor deactivation dynamics primarily associated with the backbone motif, and reveal that the competition between alternate deactivation pathways can be controlled structurally by weakening π conjugation across the backbone (e.g. by introducing steric perturbations to pi-pi interactions).

ASSOCIATED CONTENT

Supporting Information

The Supporting Information is available free of charge: Synthetic details and characterization for **TT2-Th**; additional transient absorption data and analysis.

AUTHOR INFORMATION

Corresponding Author

Email: artbragg@jhu.edu

ORCID

Nicholas P. Adams

Arthur E. Bragg: 0000-0002-3376-5494

Neal Haldar: 0000-0002-6106-4476

Chana R. Honick: 0000-0003-0005-7018

Luke R. O'Connor: 0000-0002-6406-7605

Yuqi Song: 0009-0008-0505-5402

John D. Tovar: 0000-0002-9650-2210

ACKNOWLEDGEMENTS

Photophysical and synthetic aspects of this work were supported by the National Science Foundation (CHE-2305009). C. R. H. acknowledges support from the Harry and Cleio Greer Fellowship (JHU). N. P. A. acknowledges support from the William Hooper Grafflin Fellowship (JHU). N. H. as supported by a stipend from the SEED Scholars Honors Program, U.C. Berkeley.

References Cited

1. Hohmann-Marriott, M. F.; Blankenship, R. E., Evolution of photosynthesis. *Annu. Rev. Plant Biol.* **2011**, *62*, 515-548.

2. Tochitsky, I.; Kienzler, M. A.; Isacoff, E.; Kramer, R. H., Restoring Vision to the Blind with Chemical Photoswitches. *Chem. Rev.* **2018**, *118*, 10748-10773.

3. Engelsen, O., The relationship between ultraviolet radiation exposure and vitamin D status. *Nutrients* **2010**, *2*, 482-495.

4. Goulet-Hanssens, A.; Eisenreich, F.; Hecht, S., Enlightening Materials with Photoswitches. *Adv. Mater.* **2020**, *32*, 1905966.

5. Irie, M.; Fukaminato, T.; Matsuda, K.; Kobatake, S., Photochromism of Diarylethene Molecules and Crystals: Memories, Switches, and Actuators. *Chem. Rev.* **2014**, *114*, 12174-12277.

6. Walden, S. L.; Nguyen, P. H. D.; Li, H.-K.; Liu, X.; Le, M. T. N.; Xian Jun, L.; Barner-Kowollik, C.; Truong, V. X., Visible light-induced switching of soft matter materials properties based on thioindigo photoswitches. *Nat. Comm.* **2023**, *14*, 8298.

7. Thaggard, G. C.; Haimerl, J.; Park, K. C.; Lim, J.; Fischer, R. A.; Maldeni Kankanamalage, B. K. P.; Yarbrough, B. J.; Wilson, G. R.; Shustova, N. B., Metal–Photoswitch Friendship: From Photochromic Complexes to Functional Materials. *J. Am. Chem. Soc.* **2022**, *144*, 23249-23263.

8. Gilat, S. L.; Kawai, S. H.; Lehn, J.-M., Light-Triggered Molecular Devices: Photochemical Switching Of optical and Electrochemical Properties in Molecular Wire Type Diarylethene Species. *Chem. Eur. J.* **1995**, *1*, 275-284.

9. Li, Z.; Zeng, X.; Gao, C.; Song, J.; He, F.; He, T.; Guo, H.; Yin, J., Photoswitchable diarylethenes: From molecular structures to biological applications. *Coord. Chem. Rev.* **2023**, *497*, 215451.

10. Mao, Y.; Yi, T., Fluorescent Switchable Diarylethene Derivatives and Their Application to the Imaging of Living Cells. In *Photon-Working Switches*, Yokoyama, Y.; Nakatani, K., Eds. Springer Japan: Tokyo, 2017; pp 133-152.

11. Nakashima, T.; Tsuchie, K.; Kanazawa, R.; Li, R.; Iijima, S.; Galangau, O.; Nakagawa, H.; Mutoh, K.; Kobayashi, Y.; Abe, J., et al., Self-Contained Photoacid Generator Triggered by Photocyclization of Triangle Terarylene Backbone. *J. Am. Chem. Soc.* **2015**, *137*, 7023-7026.

12. He, J.; He, J.; Wang, T.; Zeng, H., Ion-induced cycle opening of a diarylethene and its application on visual detection of Cu2+ and Hg2+ and keypad lock. *J. Mater. Chem. C* **2014**, *2*, 7531-7540.

13. Babazadeh-Mamaqani, M.; Roghani-Mamaqani, H.; Abdollahi, A.; Salami-Kalajahi, M., Optical Chemosensors based on Spiropyran-Doped Polymer Nanoparticles for Sensing pH of Aqueous Media. *Langmuir* **2022**, *38*, 9410-9420.

14. Neilson, B. M.; Lynch, V. M.; Bielawski, C. W., Photoswitchable N-Heterocyclic Carbenes: Using Light to Modulate Electron-Donating Properties. *Angew. Chem. Int. Ed.* **2011**, *50*, 10322-10326.

15. Whalley, A. C.; Steigerwald, M. L.; Guo, X.; Nuckolls, C., Reversible Switching in Molecular Electronic Devices. *J. Am. Chem. Soc.* **2007**, *129*, 12590-12591.

16. Saes, B. W. H.; Wienk, M. M.; Janssen, R. A. J., Photochromic organic solar cells based on diarylethenes. *RSC Advances* **2020**, *10*, 30176-30185.

17. Milder, M. T. W.; Areephong, J.; Feringa, B. L.; Browne, W. R.; Herek, J. L., Photoswitchable molecular wires: From a sexithiophene to a dithienylethene and back. *Chem. Phys. Lett.* **2009**, *479*, 137-139.

18. Terao, F.; Morimoto, M.; Irie, M., Light-Driven Molecular-Crystal Actuators: Rapid and Reversible Bending of Rodlike Mixed Crystals of Diarylethene Derivatives. *Angew. Chem. Int. Ed.* **2012**, *51*, 901-904.

19. Adams, N.; Tovar, J., Torsional influences on cross-conjugated thieno[3,4- b]thiophene photochromes. *J. Phys. Org. Chem.* **2024**, e4650.

20. Peters, G. M.; Tovar, J. D., Pendant Photochromic Conjugated Polymers Incorporating a Highly Functionalizable Thieno[3,4-b]thiophene Switching Motif. *J. Am. Chem. Soc.* **2019**, *141*, 3146-3152.

21. Bandara, H. M. D.; Burdette, S. C., Photoisomerization in different classes of azobenzene. *Chem. Soc. Rev.* **2012**, *41*, 1809-1825.

22. Waldeck, D. H., Photoisomerization dynamics of stilbenes. *Chem. Rev.* **1991**, *91*, 415-436.

23. Irie, M., Diarylethenes for Memories and Switches. *Chem. Rev.* **2000**, *100*, 1685-1716.

24. Kortekaas, L.; Browne, W. R., The evolution of spiropyran: fundamentals and progress of an extraordinarily versatile photochrome. *Chem. Soc. Rev.* **2019**, *48*, 3406-3424.

25. Yokoyama, Y.; Gushiken, T.; Ubukata, T., Fulgides and Related Compounds. In *Molecular Switches*, Feringa, B. L.; Browne, W. R., Eds. Wiley: 2011; pp 81-95.

26. Huang, C.-Y.; Bonasera, A.; Hristov, L.; Garmshausen, Y.; Schmidt, B. M.; Jacquemin, D.; Hecht, S., N,N′-Disubstituted Indigos as Readily Available Red-Light Photoswitches with Tunable Thermal Half-Lives. *J. Am. Chem. Soc.* **2017**, *139*, 15205-15211.

27. Irie, M.; Mohri, M., Thermally irreversible photochromic systems. Reversible photocyclization of diarylethene derivatives. *J. Org. Chem.* **1988**, *53*, 803-808.

28. Hanazawa, M.; Sumiya, R.; Horikawa, Y.; Irie, M., Thermally irreversible photochromic systems. Reversible photocyclization of 1,2-bis (2-methylbenzo[b]thiophen-3-yl)perfluorocyclocoalkene derivatives. *J. Chem. Soc., Chem. Commun.* **1992**, 206-207.

29. Herder, M.; Schmidt, B. M.; Grubert, L.; Patzel, M.; Schwarz, J.; Hecht, S., Improving the Fatigue Resistance of Diarylethene Switches. *J. Am. Chem. Soc.* **2015**, *137*, 2738-2747.

30. Irie, M.; Sakemura, K.; Okinaka, M.; Uchida, K., Photochromism of Dithienylethenes with Electron-Donating Substituents. *J. Org. Chem.* **1995**, *60*, 8305-8309.

31. Morimitsu, K.; Kobatake, S.; Irie, M., Control of Cycloreversion Quantum Yields of Diarylethenes by Introduction of Substituents at the Reactive Carbons. *Mol. Cryst. Liq. Cryst.* **2005**, *431*, 451-454.

32. Pariani, G.; Quintavalla, M.; Colella, L.; Oggioni, L.; Castagna, R.; Ortica, F.; Bertarelli, C.; Bianco, A., New Insight into the Fatigue Resistance of Photochromic 1,2-Diarylethenes. *J. Phys. Chem. C* **2017**, *121*, 23592-23598.

33. Xi, H.; Li, M.; Li, W.; Zhu, W.-H., Sterically hindered diarylethenes with thienopyridine: Substituent position effect on photochromic properties. *Dyes Pigm.* **2020**, *182*, 108620.

34. Ishibashi, Y.; Umesato, T.; Kobatake, S.; Irie, M.; Miyasaka, H., Femtosecond Laser Photolysis Studies on Temperature Dependence of Cyclization and Cycloreversion Reactions of a Photochromic Diarylethene Derivative. *J. Phys. Chem. C* **2012**, *116*, 4862-4869.

35. Nakamura, S.; Kobayashi, T.; Takata, A.; Uchida, K.; Asano, Y.; Murakami, A.; Goldberg, A.; Guillaumont, D.; Yokojima, S.; Kobatake, S., et al., Quantum yields and potential energy surfaces: a theoretical study. *J. Phys. Org. Chem.* **2007**, *20*, 821-829.

36. Valley, D. T.; Hoffman, D. P.; Mathies, R. A., Reactive and unreactive pathways in a photochemical ring opening reaction from 2D femtosecond stimulated Raman. *Phys. Chem. Chem. Phys.* **2015**, *17*, 9231-9240.

37. Asano, Y.; Murakami, A.; Kobayashi, T.; Goldberg, A.; Guillaumont, D.; Yabushita, S.; Irie, M.; Nakamura, S., Theoretical Study on the Photochromic Cycloreversion Reactions of Dithienylethenes; on the Role of the Conical Intersections. *J. Am. Chem. Soc.* **2004**, *126*, 12112-12120.

38. Mori, K.; Ishibashi, Y.; Matsuda, H.; Ito, S.; Nagasawa, Y.; Nakagawa, H.; Uchida, K.; Yokojima, S.; Nakamura, S.; Irie, M., et al., One-Color Reversible Control of Photochromic Reactions in a Diarylethene Derivative: Three-Photon Cyclization and Two-Photon Cycloreversion by a Near-Infrared Femtosecond Laser Pulse at 1.28 μm. *J. Am. Chem. Soc.* **2011**, *133*, 2621-2625.

39. Sotome, H.; Nagasaka, T.; Une, K.; Okui, C.; Ishibashi, Y.; Kamada, K.; Kobatake, S.; Irie, M.; Miyasaka, H., Efficient Cycloreversion Reaction of a Diarylethene Derivative in Higher Excited States Attained by Off-Resonant Simultaneous Two-Photon Absorption. *J. Phys. Chem. Lett.* **2017**, *8*, 3272-3276.

40. Ward, C. L.; Elles, C. G., Controlling the Excited-State Reaction Dynamics of a Photochromic Molecular Switch with Sequential Two-Photon Excitation. *J. Phys. Chem. Lett.* **2012**, *3*, 2995-3000.

41. Ward, C. L.; Elles, C. G., Cycloreversion Dynamics of a Photochromic Molecular Switch via One-Photon and Sequential Two-Photon Excitation. *J. Phys. Chem. A* **2014**, *118*, 10011-10019.

42. Honick, C. R.; Peters, G. M.; Young, J. D.; Tovar, J. D.; Bragg, A. E., Core structure dependence of cycloreversion dynamics in diarylethene analogs. *Phys. Chem. Chem. Phys.* **2020**, *22*, 3314-3328.

43. Nie, H.; Schauser, N. S.; Dolinski, N. D.; Geng, Z.; Oh, S.; Chabinyc, M. L.; Hawker, C. J.; Segalman, R. A.; Read de Alaniz, J., The role of anions in light-driven conductivity in diarylethene-containing polymeric ionic liquids. *Polym. Chem.* **2021**, *12*, 719-724.

44. Patel, D. G.; Walton, I. M.; Cox, J. M.; Gleason, C. J.; Butzer, D. R.; Benedict, J. B., Photoresponsive porous materials: the design and synthesis of photochromic diarylethene-based linkers and a metal–organic framework. *Chem. Commun.* **2014**, *50*, 2653-2656.

45. Williams, D. E.; Rietman, J. A.; Maier, J. M.; Tan, R.; Greytak, A. B.; Smith, M. D.; Krause, J. A.; Shustova, N. B., Energy transfer on demand: photoswitch-directed behavior of metal-porphyrin frameworks. *J. Am. Chem. Soc.* **2014**, *136*, 11886-11889.

46. Jung, I.; Choi, H.; Kim, E.; Lee, C.-H.; Kang, S. O.; Ko, J., Synthesis and photochromic reactivity of macromolecules incorporating four dithienylethene units. *Tetrahedron* **2005**, *61*, 12256-12263.

47. Luo, Q.; Cheng, H.; Tian, H., Recent progress on photochromic diarylethene polymers. *Polym. Chem.* **2011**, *2*, 2435-2443.

48. Kawai, T.; Kunitake, T.; Irie, M., Novel Photochromic Conducting Polymer Having Diarylethene Derivative in the Main Chain. *Chem. Lett.* **2003**, *28*, 905-906.

49. Kim, E.; Lee, H. W., Photo-induced electrical switching through a mainchain polymer. *J. Mater. Chem.* **2006**, *16*, 1384-1389.

50. Choi, H.; Lee, H.; Kang, Y.; Kim, E.; Kang, S. O.; Ko, J., Photochromism and Electrical Transport Characteristics of a Dyad and a Polymer with Diarylethene and Quinoline Units. *J. Org. Chem.* **2005**, *70*, 8291-8297.

51. Perrier, A.; Maurel, F.; Jacquemin, D., Interplay Between Electronic and Steric Effects in Multiphotochromic Diarylethenes. *J. Phys. Chem. C* **2011**, *115*, 9193-9203.

52. Molloy, M. S.; Snyder, J. A.; Bragg, A. E., Structural and Solvent Control of Nonadiabatic Photochemical Bond Formation: Photocyclization of o-Terphenyl in Solution. *J. Phys. Chem. A* **2014**, *118*, 3913-3925.

53. Schmidhammer, U.; Jeunesse, P.; Stresing, G.; Mostafavi, M., A broadband ultrafast transient absorption spectrometer covering the range from near-infrared (NIR) down to green. *Appl. Spectrosc.* **2014**, *68*, 1137-1147.

54. van Stokkum, I. H.; Larsen, D. S.; van Grondelle, R., Global and target analysis of time-resolved spectra. *Biochim. Biophys. Acta* **2004**, *1657*, 82-104.

55. Lebedev, M. V.; Misochko, O. V.; Dekorsy, T.; Georgiev, N., On the nature of “coherent artifact”. *J. Exp. Theor. Phys.* **2005**, *100*, 272-282.

56. Snyder, J. A.; Bragg, A. E., Ultrafast Pump–Repump–Probe Photochemical Hole Burning as a Probe of Excited-State Reaction Pathway Branching. *J. Phys. Chem. Lett.* **2018**, *9*, 5847-5854.

57. Matsuda, K., Photoswitching of Intramolecular Magnetic Interaction Using Diarylethene Photochromic Spin Couplers. *Bull. Chem. Soc. Jpn.* **2005**, *78*, 383-392.

58. Pu, S.; Zheng, C.; Le, Z.; Liu, G.; Fan, C., Substituent effects on the properties of photochromic diarylethenes. *Tetrahedron* **2008**, *64*, 2576-2585.

59. Irie, M.; Miyatake, O.; Uchida, K.; Eriguchi, T., Photochromic Diarylethenes with Intralocking Arms. *J. Am. Chem. Soc.* **1994**, *116*, 9894-9900.

60. Paa, W.; Yang, J. P.; Rentsch, S., Ultrafast intersystem crossing in thiophene oligomers investigated by fs-pump-probe spectroscopy. *Synth. Met.* **2001**, *119*, 525-526.

61. Gratz, H.; Penzkofer, A., Triplet–triplet absorption of some organic molecules determined by picosecond laser excitation and time-delayed picosecond light continuum probing. *J. Photochem. Photobiol. A - Chem* **1999**, *127*, 21-30.